JOURNAL OF SYNCHROTRON RADIATION

ISSN 1600-5775

Received 12 September 2017
Accepted 26 October 2017

Edited by E. Plönjes, DESY, Germany

Keywords: free-electron laser; XUV pulse duration diagnostic; transient grating spectroscopy.

Characterization of ultrafast free-electron laser pulses using extreme-ultraviolet transient gratings

F. Capotondi,* L. Foglia, M. Kiskinova, C. Masciovecchio, R. Mincigrucci, D. Naumenko, E. Pedersoli, A. Simoncig and F. Bencivenga

Elettra-Sincrotrone Trieste SCpA, SS 14 km 163.5 in Area Science Park, I-34012 Basovizza, Trieste, Italy. *Correspondence e-mail: flavio.capotondi@elettra.eu

The characterization of the time structure of ultrafast photon pulses in the extreme-ultraviolet (EUV) and soft X-ray spectral ranges is of high relevance for a number of scientific applications and photon diagnostics. Such measurements can be performed following different strategies and often require large setups and rather high pulse energies. Here, high-quality measurements carried out by exploiting the transient grating process, *i.e.* a third-order non-linear process sensitive to the time-overlap between two crossed EUV pulses, is reported. From such measurements it is possible to obtain information on both the second-order intensity autocorrelation function and on the coherence length of the pulses. It was found that the pulse energy density needed to carry out such measurements on solid state samples can be as low as a few mJ cm^{-2}. Furthermore, the possibility to control the arrival time of the crossed pulses independently might permit the development of a number of coherent spectroscopies in the EUV and soft X-ray regime, such as, for example, photon echo and two-dimensional spectroscopy.

1. Introduction

The cutting-edge research opportunities opened up by the increasing number of free-electron laser (FEL) facilities (Emma *et al.*, 2010; Feldhaus, 2010; Allaria *et al.*, 2012; Ishikawa *et al.*, 2012), providing extreme-ultraviolet (EUV) and X-ray femtosecond pulses, calls for the promotion of ultrafast methodologies, until now limited to the realms of table-top optical lasers. Among others, in recent years several experimental approaches have been developed to determine the temporal duration of sub-picosecond short-wavelength radiation pulses (Gahl *et al.*, 2008; Maltezopoulos *et al.*, 2008; Mitzner *et al.*, 2009; Moshammer *et al.*, 2011; Lutman *et al.*, 2012; Riedel *et al.*, 2013; Behrens *et al.*, 2014; Helml *et al.*, 2014; Düsterer *et al.*, 2014). Such tools can be used both for scientific applications and time-domain photon diagnostics, the latter being one of the major challenges for the novel field of ultrafast X-ray science. Indeed, precise knowledge of the temporal profile of sub-picosecond pulses is of paramount importance in dynamical studies, since it defines the temporal resolution of the experiment and determines the distribution of the pulse energy inside the sample. Among various methods for time-domain diagnostics, those based on autocorrelation approaches are commonly and widely used in the optical regime (Roth *et al.*, 2002; Diels & Rudolph, 2006; Walmsley & Dorrer, 2009; Danailov *et al.*, 2015; Gaižauskas *et al.*, 2016). Most of them rely on non-linear processes (*e.g.* second-harmonic generation) sensitive to the temporal overlap between two identical replica of the same pulse.

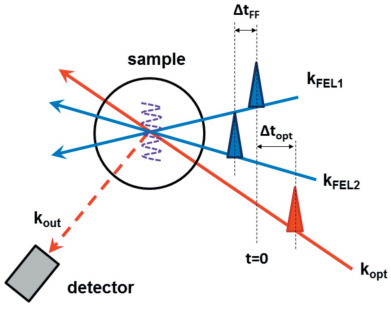

In contrast to the relative simplicity of optical autocorrelation, EUV/X-ray autocorrelation requires large experimental apparatuses, such as split-and-delay units or EUV interferometers (Mitzner *et al.*, 2009; Jiang *et al.*, 2010; Moshammer *et al.*, 2011; Wöstmann *et al.*, 2013), and often needs high photon fluxes (about a few J cm^{-2}). The main limitation in the autocorrelation technique in the EUV/X-ray regime is the lack of specific non-linear processes providing a sufficient signal-to-noise ratio at low FEL intensity. Indeed, most of the aforementioned EUV/X-ray autocorrelation experiments (Mitzner *et al.*, 2009; Jiang *et al.*, 2010; Moshammer *et al.*, 2011) have been performed with gas phase samples, monitoring the yield of multiply ionized atoms or molecules generated by non-sequential absorption of n photons. Such processes are intrinsically inefficient, since the multiple ionization cross section has an unfavorable power-law dependence on the number of absorbed photons. A considerably large power density ($\sim 10^{14}$ to 10^{15} W cm^{-2}) is necessary to observe such signals from gas phase samples. More efficient processes to characterize the time profile of ultrafast EUV/X-ray pulses *via* autocorrelation methods are strongly desirable in the emerging field of ultrafast X-ray science as on-line diagnostics. This need calls for using solid state targets that can provide more intense non-linear signals due to the larger atomic density. However, the exploitation of the non-linear wave-mixing process in the EUV/X-ray regime is just the very beginning (Glover *et al.*, 2012; Shwartz *et al.*, 2014; Bencivenga *et al.*, 2015; Fuchs *et al.*, 2015) but it is growing fast thanks to the availability of high-brightness FEL sources. In particular, the seeded FEL FERMI (Allaria *et al.*, 2012, 2013*a*) has been used to demonstrate the feasibility of the EUV/soft X-ray transient grating (XTG) approach (Bencivenga *et al.*, 2015, 2016). This particular kind of four-wave-mixing process uses two identical crossed FEL pulses to excite the sample, imposing a controlled spatial modulation, with a time profile equal to those of the excitation pulses (Bloembergen, 1982; Dhar *et al.*, 1994; Mukamel, 1995). The sample response can be monitored by an optical (probing) laser pulse, which is diffracted by the excited spatial periodicity of the sample. By measuring the total intensity of the diffracted optical beam (XTG signal) as a function of the time delay ($\Delta t_{\rm opt}$) between the optical probe and the two crossed FEL pulses one can access various kinds of sample dynamics (Dadusc *et al.*, 2001; Foster *et al.*, 2006; Avisar & Tannor, 2011). In this case, the $\Delta t_{\rm opt}$ dependence of the measured signal is related to the intrinsic sample dynamics and the time resolution is given by the cross correlation of the input pulses. On the other hand, when the optical laser pulse is tuned at $\Delta t_{\rm opt} = 0$, the response of the system is essentially 'instantaneous' and is given by the third-order polarization. Under such conditions, a scan of the time-delay ($\Delta t_{\rm FF}$; see Fig. 1 for the definition of pulses and delays) between the two crossed FEL beams while looking at the XTG signal gives access to the second-order intensity autocorrelation function and to the coherence length of the FEL (pump) pulses (Nighan Jr *et al.*, 1988). The two quantities overlap in the case of pulses close to the Fourier transform limit, such as those generated by

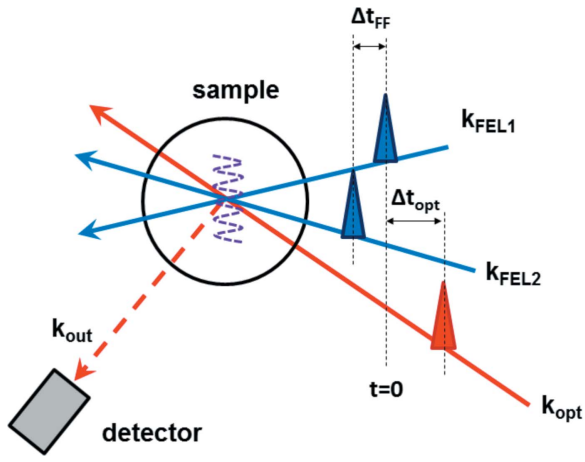

Figure 1
Sketch of the XTG experiment, where the optical and FEL pulses are labelled as $\mathbf{k}_{\rm opt}$ (full red line) and $\mathbf{k}_{\rm FEL1,2}$ (full blue lines), respectively, while the signal field ($\mathbf{k}_{\rm out}$) is indicated with the dashed red line. The relevant delays ($\Delta t_{\rm opt}$ and $\Delta t_{\rm FF}$) are shown as well. Time-zero conditions ($T = 0$) are assumed to coincide with the arrival time at the sample of the FEL pulse labelled as $\mathbf{k}_{\rm FEL1}$.

FERMI (Allaria *et al.*, 2012). Within this frame we hereafter assume that the measured XTG signal *versus* $\Delta t_{\rm FF}$ can be identified with the autocorrelation function of the FEL pulses, an assumption *a posteriori* endorsed by the almost perfect single Gaussian lineshape of the experimental signal. It is worth mentioning that, in sources with a lower degree of longitudinal coherence, an interferometric approach (*i.e.* directly measuring the fringe visibility of the intensity grating) was successfully applied to determine the coherence length of the radiation (Mitzner *et al.*, 2008; Schlotter *et al.*, 2010). In such cases, the signal was dominated by the so-called 'coherent spike' because of the sensitivity of the XTG to the source coherence properties (Nighan Jr *et al.*, 1988). This highlights how XTG-based methods can provide useful information to characterize the temporal properties of ultrafast FEL pulses in different regimes.

2. Experimental details

The experiment was carried out using the mini-TIMER setup at the DiProI endstation (Capotondi *et al.*, 2013, 2015) of the FERMI facility. The system was placed inside the main vacuum vessel and consists of a compact delay-line able to split the FEL beam into two halves and recombine them with a given crossing angle (2θ) and time delay ($\Delta t_{\rm FF}$) at the sample. Fig. 2(*a*) shows a sketch (top view) of the experimental setup. A planar C-coated mirror (M_0) is used to divide the FEL wavefront into two halves. The reflected beam is directed towards a second mirror (M_2), while the mirror M_1 reflects the direct half-beam towards the sample position. Each of the three mirrors is mounted on a fully encoded four-axis piezoelectric stage that allows controlling the X, Z, pitch and roll positions [see Fig. 2(*a*) for the reference frame]. Focusing of the FEL beam is realised using adaptive Kirkpatrick–Baez optics, placed upstream of the endstation (1.8 m from the

sample position) and capable of flexibly setting the FEL spot size at the sample (Raimondi *et al.*, 2013). In the standard XTG configuration the three mirrors are parallel, M_1 and M_2 have the same Z positions and the M_0–M_1 distance (L = 125 mm) equals the M_2–sample distance. The two crossed FEL beams generate a modulation on the sample along the X direction with a spatial periodicity $L_{XTG} = \lambda_{FEL}/2\sin(2\theta/2)$, where λ_{FEL} is the FEL wavelength. The dynamics stimulated by the XTG are then monitored by an optical probe pulse, impinging on the sample at an angle of incidence of about 45° with a time delay Δt_{opt}. This imposes some constraints on the exploitable (λ_{FEL}, 2θ)-range, which must correspond to L_{XTG} values that match the diffraction condition for the optical probe. The correctness of such conditions was checked by monitoring the beam on a scintillator screen placed at the sample position (spatial overlap) and *via* cross-correlation measurements (temporal overlap), based on transient optical reflectivity from a reference sample (Danailov *et al.*, 2014; Casolari *et al.*, 2014).

The presence of encoders in all system axes permits the application of a controlled delay between the two FEL pulses, maintaining constant their spatial overlap and crossing angle. This condition ensures that the emission angle of the XTG signal is independent of Δt_{FF}. In order to perform Δt_{FF} scans, three motions of the mirrors with respect to the standard XTG configuration are necessary [see Figs. 2(*a*) and 2(*b*)], *i.e.* the Z position of M_2 (hereafter referred to as ΔZ) and the pitch angles of both M_0 and M_2 (hereafter referred to as $\Delta\alpha$). The latter are moved by the same amount in order to keep 2θ fixed, and this amount is determined by the constraint of keeping the same impinging point on the M_2 mirror as a function of ΔZ. This leads to the following equation,

$$\Delta\alpha = \theta - \frac{1}{2}\tan^{-1}\left[L\tan(2\theta)/(L-\Delta Z)\right]. \quad (1)$$

Using equation (1), after some straightforward trigonometrical calculations one can determine the value of Δt_{FF}, which is given by

$$\Delta t_{FF} = c^{-1}\left(\left\{(L+\Delta Z)^2 + \left[L\tan(2\theta)\right]^2\right\}^{1/2} - \left[L/\cos(2\theta) + \Delta Z\right]\right), \quad (2)$$

where c is the speed of light in a vacuum. We finally note that the pivot of the M_0 pitch is kept fixed on the mirror edge that is responsible for the beam splitting, as sketched in Fig. 2(*a*).

Fig. 2(*b*) shows the theoretical values of Δt_{FF} *versus* ΔZ for different values of 2θ, in the 2°–6° range, which was already exploited in XTG experiments, so far carried out in a λ_{FEL} range of about 30–10 nm. Due to the grazing-angle geometry, a very high accuracy on Δt_{FF} can be obtained. For example, at $2\theta = 6°$, a 50 µm change in ΔZ correspond to just 1 fs variation in Δt_{FF}, allowing for the realisation of ultra-precise FEL autocorrelation measurements. Actually, it is worth noting that the mechanical precision of the translational and rotational stages in principle allows for Δt_{FF} steps as short as 0.005 fs, though other experimental aspects, such as for example the wavefront tilt between FEL pulses, limits the resolution of the measurements to the femtosecond regime. Indeed, the crossed FEL pulses are expected to show a temporal broadening of the order of $\sigma_p\sin(2\theta)/c$, where σ_p is the probe beam waist at the sample projected along the grating vector, which during the measurements has to be kept smaller than the pump beam.

In the present experiment we used λ_{FEL} = 26.1 nm, while the probe pulse was the second harmonic (λ_{opt} = 393 nm, about 150 fs FWHM) of a Ti:sapphire laser. The focal spot areas of FEL and laser beams were set to 120 µm × 120 µm and 60 µm × 60 µm (FWHM), respectively, while 2θ = 5.5°. Under these conditions the spatial periodicity of the XTG ($L_{XTG} \simeq 275$ nm) is sufficiently large to diffract the optical probe at about 48°. The XTG signal was then collected by a CCD detector placed at 150 mm from the sample plane [see also Fig. 2(*a*)]. The experimental time resolution in Δt_{FF} scans is essentially determined by the finite value of 2θ and by the dimensions of the probe beam waist; this leads to a temporal

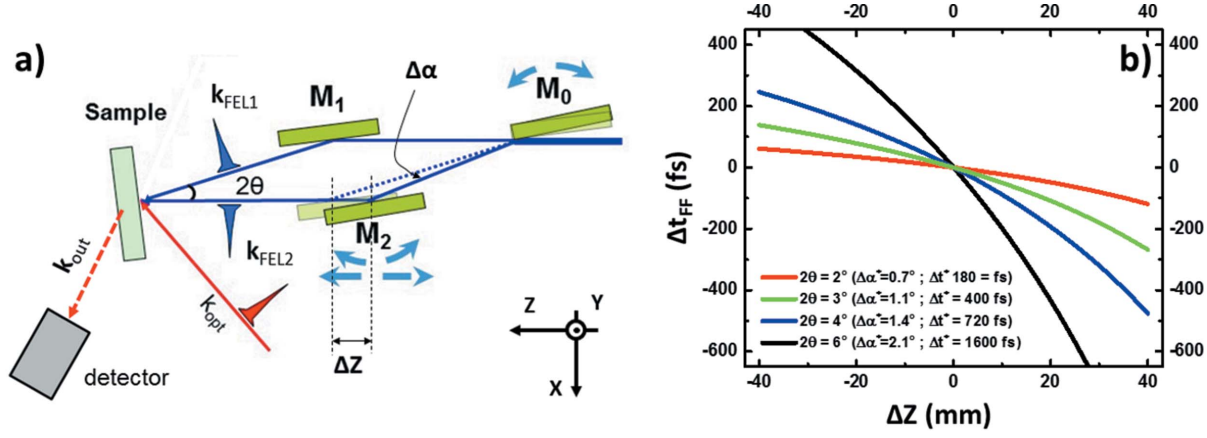

Figure 2
(*a*) Sketch of the (ΔZ, $\Delta\alpha$) movement needed to scan Δt_{FF} (angles are exaggerated for clarity); the reference frame is shown in the bottom right-hand corner. (*b*) Dependence of Δt_{FF} on ΔZ for typical values of 2θ, reported in the figure legend; the total ranges in Δt_{FF} (Δt^*) and $\Delta\alpha$ ($\Delta\alpha^*$) are indicated in parentheses (for a ΔZ range of −40 mm to +40 mm).

broadening of about 20 fs, which has been deconvoluted from the measured line profile.

3. Results and discussion

Fig. 3(*a*) shows an example of a XTG signal from a diamond sample, collected by setting $\Delta t_{FF} = 0$ and scanning Δt_{opt}. The data were acquired using a FEL intensity of 1 µJ, corresponding to an average energy flux deposited on the sample of about 2.5 mJ cm^{-2} per pulse. For each time-delay point the XTG signal intensity on the detector was integrated over 300 FEL shots (the FEL repetition rate was 50 Hz). In order to remove the residual background on the CCD image, mainly due to spurious scattering of the optical probe, we subtract from the raw data image a background image collected using the same exposure time but closing with a mechanical shutter the FEL radiation.

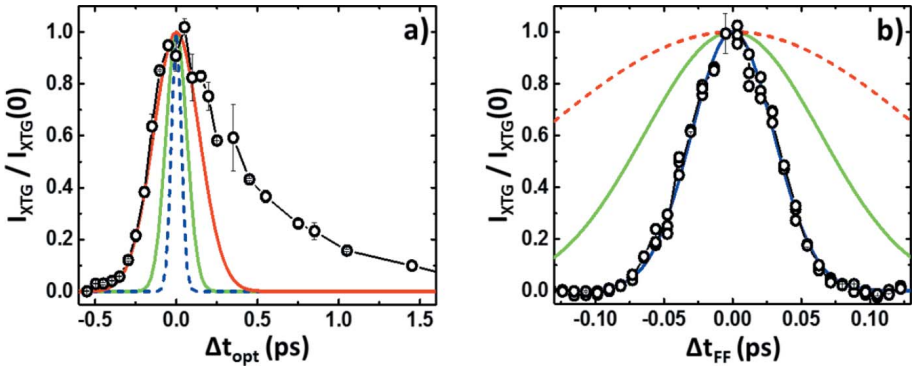

Figure 3
(*a*) XTG data obtained by scanning Δt_{opt} at $\Delta t_{FF} = 0$; the rise time of the signal can be associated with the FEL–optical cross correlation while the decay is related to some specific sample dynamics. (*b*) XTG data obtained by scanning Δt_{FF} at $\Delta t_{opt} = 0$, that can be associated with the FEL autocorrelation. Red, blue and green curves are Gaussian functions with FWHM of 330 fs, 70 fs and 150 fs, respectively, where the latter is representative of the optical pulse duration.

The dependence of the XTG signal on Δt_{opt} is markedly asymmetric and features a Gaussian-like rise at negative delays with a FWHM of about 330 fs [red Gaussian curve in Fig. 3(*a*)] followed by a much longer decay at positive delays. The signal rise is compatible with the convolution between the FEL and optical pulses. It is essentially dominated by the large wavefront tilt between the optical and FEL pulses and substantially longer that the estimated time duration of the FEL pulse (~50–60 fs) (De Ninno *et al.*, 2015; Finetti *et al.*, 2017). For $\Delta t_{opt} > 0$ the XTG signal decays *via* different mechanisms, which include complex relaxation dynamics involving both electronic and lattice excitations (Medvedev *et al.*, 2013; Ziaja *et al.*, 2013). Indeed, hot electrons excited in the conduction band relax *via* electron–electron scattering on the femtosecond scale and electron–phonon scattering on the picosecond time scale. Then, such an electronic excitation grating turns into a thermal grating, which relaxes on the hundreds of picoseconds scale, and, depending on the specific sample, can be accompanied by strain and/or molecular vibration gratings, which typically show time domain oscillations related to optical and acoustic phonons (Bencivenga *et al.*, 2015). On the other hand, Fig. 3(*b*) shows the XTG signal collected by fixing $\Delta t_{opt} = 0$ and by scanning Δt_{FF}. The XTG signal is now symmetric and considerably faster compared with the data reported in Fig. 3(*a*). This suggests that such a signal is essentially due to the almost instantaneous electronic response of the non-linear polarization responsible for the XTG generation. A Gaussian fit of the experimental data (blue curves in Figs. 3 and 4) indicates a FWHM of 70–85 fs, which is consistent with a FEL pulse duration of about 50–

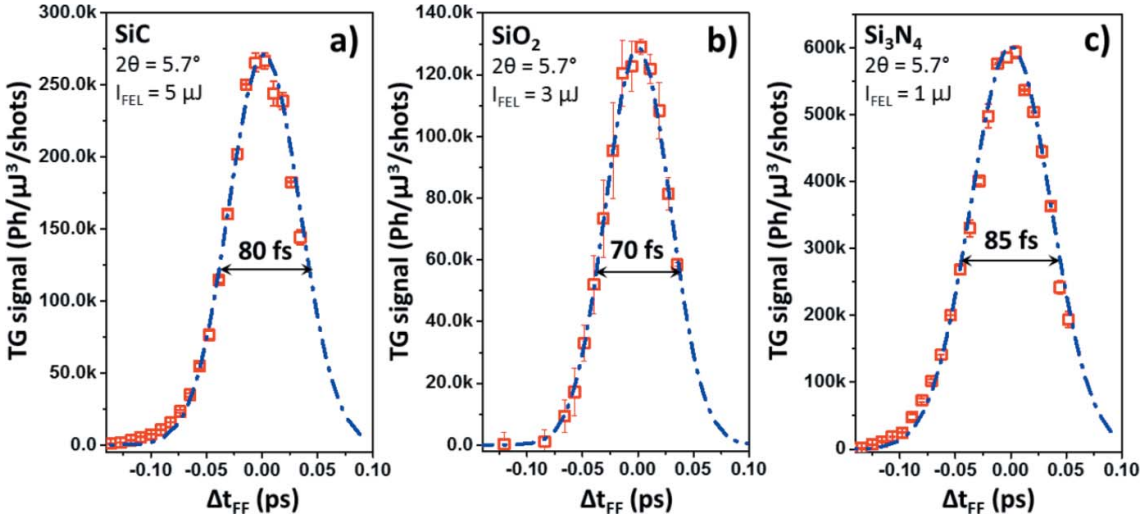

Figure 4
XTG data obtained by scanning Δt_{FF} at $\Delta t_{opt} = 0$ on SiC (*a*), SiO_2 (*b*) and Si_3N_4 (*c*). The blue lines are Gaussian functions with FWHM as indicated in the figure. The experimental conditions are synthetically reported in the figure legend; the parameters that are not indicated are the same used in the case of diamond (see text).

60 fs, in good agreement with both theoretical expectations (Ratner *et al.*, 2012) and experimental findings obtained at FERMI in the same range of wavelengths (Finetti *et al.*, 2017).

Similar results, as reported in Fig. 4, were obtained with other samples (namely SiO_2, thin membranes of Si_3N_4 and SiC) at a slightly different FEL wavelength (λ_{FEL} = 27.6 nm), hence showing the general applicability of this approach to various solid state samples. XTG data are reported in units of detected photons per pulse per μJ^3 in order to highlight the different strength of the XTG response (the focal spot size at the sample for both FEL and optical beams was nearly the same as for the data in Fig. 3). For these measurements the stroke of ΔZ was limited by a mechanical conflict in the setup, occasionally occurred during this specific experimental run.

Unfortunately, we could not exploit disparate experimental conditions (*e.g.* crossing angles, focal spot size, wavelength and time duration of both FEL and optical pulses, *etc.*) during the investigations reported here, except for the variability in the FEL flux at the sample (I_{FEL}) and for the availability of the 'twin-seed' double FEL pulse mode. The former results, reported in Fig. 5(*a*), show how the shape of the auto-correlation profile is independent of I_{FEL} and highlight the very low flux (as low as 1.25 mJ cm^{-2}) needed to carry out such high-quality measurements, a capability essentially due to the background-free nature of the XTG approach. Though a very specialized setup is required for such measurements, the possibility to compact such a setup (in the present version it fits into a $\sim$300 mm $\times$ 200 mm in-vacuum breadboard, excluding the focusing optics) and to obtain high-quality data with a very low FEL flux could in principle permit using a small fraction of the main FEL beam to carry out temporal characterization measurements that could run in parallel with other experiments. This should potentially allow for the development of XTG-based methods in the broader context of temporal diagnostics for FEL sources (Düsterer *et al.*, 2014), though applications beyond the XUV regime (*i.e.* in the X-ray range) are hampered by the phase-matching constraint, which requires an increasingly large mismatch between the FEL crossing angle and the angle of incidence of the optical probe for decreasing FEL wavelength. This implies a reduction of the crossing angle and, therefore, a large decrease in the Δt_{FF} range (see Fig. 2*b*), which could be mitigated by a redesign of the system with larger M_0–M_1 and M_1–sample distances.

In order to underline the capability of the discussed approach to determine the time-dependence of 'structured' FEL pulses, with high accuracy and in a large time delay range, we used the twin-seed mode available at the facility (Allaria *et al.*, 2013*b*; Ferrari *et al.*, 2016), as sketched in Fig. 5(*b*), to simulate the presence of a satellite pulse well separated from the main FEL pulse. In this specific case the two pulses were separated by $\Delta t^* \simeq 270$ fs and had equal wavelength, in order to permit the generation of the XTG when the 'head' and 'tail' pulses were brought into interaction upon scanning Δt_{FF}, and the intensity ratio was purposely kept different from 1. In the present case, the delay line setup was assembled in an asymmetric way in order to extend the Δt_{FF} range in one direction. Therefore, we can record only the satellite peak at positive delay. Besides this caveat, the results, displayed in Fig. 5(*c*), clearly agree with the expectations and demonstrate how the XTG-based approach can be straightforwardly used to precisely determine the time separation between two consecutive FEL pulses, in the range of a few femtoseconds to a few hundreds of femtoseconds. Such capability can be exploited, for example, for time-diagnostics in collinear FEL-pump/FEL-probe experiments, where the FEL two-pulse sequence is generated either by split-and-delay units (Wöstmann *et al.*, 2013; Günther *et al.*, 2011) or by special operation modes of the source (Allaria *et al.*, 2013*b*; Ferrari *et al.*, 2016).

We finally stress how the XTG is a specific case in the more general framework of EUV four-wave-mixing processes, and it is inherently featured by two delays (see Fig. 1) that play

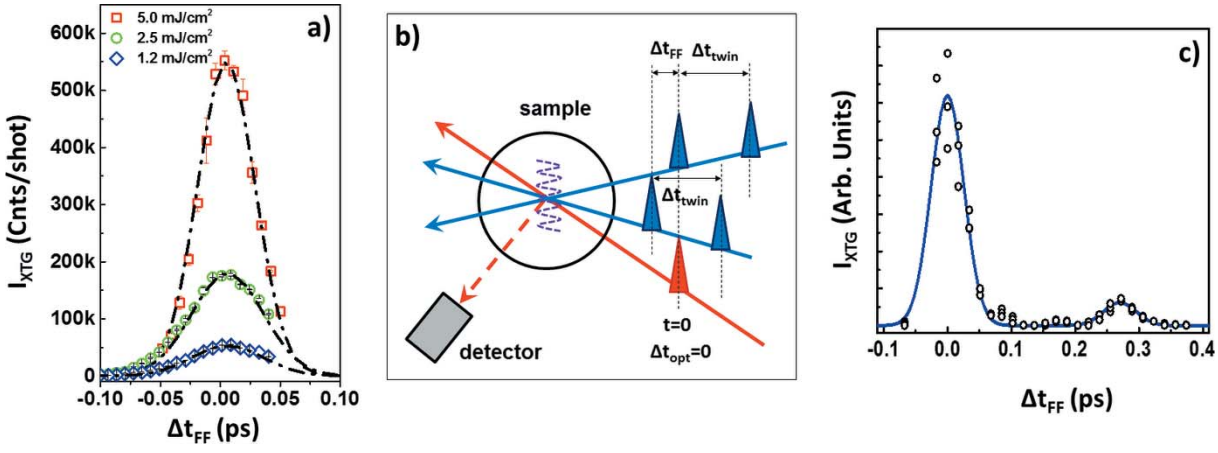

Figure 5
(*a*) XTG data obtained by scanning Δt_{FF} at Δt_{opt} = 0 on Si_3N_4 at different values of I_{FEL}, as indicated in the figure legend. (*b*) Sketch of the XTG experiment carried out in the twin-seed mode on a diamond sample; Δt^* is the time delay between the two FEL pulses. (*c*) XTG data obtained by scanning Δt_{FF} at Δt_{opt} = 0; the blue line is the sum of two Gaussian functions with FWHM of 60 fs, separated by 270 fs time delay and with a 0.1 intensity ratio.

different roles in the excitation and probing processes. Therefore, the capability to reliably control both delays provides the main experimental tool to develop two-dimensional spectroscopy in the EUV and soft X-ray regime, which is a targeted outlook for ultrafast X-ray applications (Tanaka *et al.*, 2001; Tanaka & Mukamel, 2002; Bencivenga *et al.*, 2013), with potential relevant applications in several fields across physics and chemistry disciplines.

4. Conclusions

We have shown that scanning the relative time-delay between two half FEL pulses generating the dynamic grating in a XTG experiment provides useful information about the FEL pulse duration. The method is extremely robust and can be applied to different types of solid samples commonly used as timing tools in FEL facilities. Compared with the other type of autocorrelation methods in the EUV/soft X-ray regime, based on multiple ionization of atoms or molecules in the gas phase (Mitzner *et al.*, 2009; Jiang *et al.*, 2010; Moshammer *et al.*, 2011), the XTG approach requires a lower energy density deposited on the sample (a few mJ cm^{-2}), allowing for 'on-line' timing diagnostics that can run in parallel with other experiments. Furthermore, the possibility to independently control two time-delays in the same four-wave-mixing process opens up a concrete perspective for EUV/soft X-ray two-dimensional-spectroscopy.

References

Allaria, E., Appio, R., Badano, L., Barletta, W., Bassanese, S., Biedron, S. G., Borga, A., Busetto, E., Castronovo, D., Cinquegrana, P., Cleva, S., Cocco, D., Cornacchia, M., Craievich, P., Cudin, I., D'Auria, G., Dal Forno, M., Danailov, M. B., De Monte, R., De Ninno, G., Delgiusto, P., Demidovich, A., Di Mitri, S., Diviacco, B., Fabris, A., Fabris, R., Fawley, W., Ferianis, M., Ferrari, E., Ferry, S., Froehlich, L., Furlan, P., Gaio, G., Gelmetti, F., Giannessi, L., Giannini, M., Gobessi, R., Ivanov, R., Karantzoulis, E., Lonza, M., Lutman, A., Mahieu, B., Milloch, M., Milton, S. V., Musardo, M., Nikolov, I., Noe, S., Parmigiani, F., Penco, G., Petronio, M., Pivetta, L., Predonzani, M., Rossi, F., Rumiz, L., Salom, A., Scafuri, C., Serpico, C., Sigalotti, P., Spampinati, S., Spezzani, C., Svandrlik, M., Svetina, C., Tazzari, S., Trovo, M., Umer, R., Vascotto, A., Veronese, M., Visintini, R., Zaccaria, M., Zangrando, D. & Zangrando, M. (2012). *Nat. Photon.* **6**, 699–704.

Allaria, E., Bencivenga, F., Borghes, R., Capotondi, F., Castronovo, D., Charalambous, P., Cinquegrana, P., Danailov, M. B., De Ninno, G., Demidovich, A., Di Mitri, S., Diviacco, B., Fausti, D., Fawley, W. M., Ferrari, E., Froehlich, L., Gauthier, D., Gessini, A., Giannessi, L., Ivanov, R., Kiskinova, M., Kurdi, G., Mahieu, B., Mahne, N., Nikolov, I., Masciovecchio, C., Pedersoli, E., Penco, G., Raimondi, L., Serpico, C., Sigalotti, P., Spampinati, S., Spezzani, C., Svetina, C., Trovò, M. & Zangrando, M. (2013*b*). *Nat. Commun.* **4**, 2476.

Allaria, E., Castronovo, D., Cinquegrana, P., Craievich, P., Dal Forno, M., Danailov, M. B., D'Auria, G., Demidovich, A., De Ninno, G., Di Mitri, S., Diviacco, B., Fawley, W. M., Ferianis, M., Ferrari, E., Froehlich, L., Gaio, G., Gauthier, D., Giannessi, L., Ivanov, R., Mahieu, B., Mahne, N., Nikolov, I., Parmigiani, F., Penco, G., Raimondi, L., Scafuri, C., Serpico, C., Sigalotti, P., Spampinati, S., Spezzani, C., Svandrlik, M., Svetina, C., Trovo, M., Veronese, M., Zangrando, D. & Zangrando, M. (2013*a*). *Nat. Photon.* **7**, 913–918.

Avisar, D. & Tannor, D. J. (2011). *Phys. Rev. Lett.* **106**, 170405.

Behrens, C., Decker, F. J., Ding, Y., Dolgashev, V. A., Frisch, J., Huang, Z., Krejcik, P., Loos, H., Lutman, A., Maxwell, T. J., Turner, J., Wang, J., Wang, M. H., Welch, J. & Wu, J. (2014). *Nat. Commun.* **5**, 3762.

Bencivenga, F., Baroni, S., Carbone, C., Chergui, M., Danailov, M. B., De Ninno, G., Kiskinova, M., Raimondi, L., Svetina, C. & Masciovecchio, C. (2013). *New J. Phys.* **15**, 123023.

Bencivenga, F., Calvi, A., Capotondi, F., Cucini, R., Mincigrucci, R., Simoncig, A., Manfredda, M., Pedersoli, E., Principi, E., Dallari, F., Duncan, R. A., Izzo, M. G., Knopp, G., Maznev, A. A., Monaco, G., Di Mitri, S., Gessini, A., Giannessi, L., Mahne, N., Nikolov, I. P., Passuello, R., Raimondi, L., Zangrando, M. & Masciovecchio, C. (2016). *Faraday Discuss.* **194**, 283–303.

Bencivenga, F., Cucini, R., Capotondi, F., Battistoni, A., Mincigrucci, R., Giangrisostomi, E., Gessini, A., Manfredda, M., Nikolov, I. P., Pedersoli, E., Principi, E., Svetina, C., Parisse, P., Casolari, F., Danailov, M. B., Kiskinova, M. & Masciovecchio, C. (2015). *Nature (London)*, **520**, 205–208.

Bloembergen, N. (1982). *Rev. Mod. Phys.* **54**, 685–695.

Capotondi, F., Pedersoli, E., Bencivenga, F., Manfredda, M., Mahne, N., Raimondi, L., Svetina, C., Zangrando, M., Demidovich, A., Nikolov, I., Danailov, M., Masciovecchio, C. & Kiskinova, M. (2015). *J. Synchrotron Rad.* **22**, 544–552.

Capotondi, F., Pedersoli, E., Mahne, N., Menk, R. H., Passos, G., Raimondi, L., Svetina, C., Sandrin, G., Zangrando, M., Kiskinova, M., Bajt, S., Barthelmess, M., Fleckenstein, H., Chapman, H. N., Schulz, J., Bach, J., Frömter, R., Schleitzer, S., Müller, L., Gutt, C. & Grübel, G. (2013). *Rev. Sci. Instrum.* **84**, 051301.

Casolari, F., Bencivenga, F., Capotondi, F., Giangrisostomi, E., Manfredda, M., Mincigrucci, R., Pedersoli, E., Principi, E., Masciovecchio, C. & Kiskinova, M. (2014). *Appl. Phys. Lett.* **104**, 191104.

Dadusc, G., Ogilvie, J. P., Schulenberg, P., Marvet, U. & Miller, R. J. D. (2001). *Proc. Natl Acad. Sci. USA*, **98**, 6110–6115.

Danailov, M. B., Alsous, M. B., Cinquegrana, P., Demidovich, A., Kurdi, G., Nikolov, I. & Sigalotti, P. (2015). *Appl. Phys. B*, **120**, 97–104.

Danailov, M. B., Bencivenga, F., Capotondi, F., Casolari, F., Cinquegrana, P., Demidovich, A., Giangrisostomi, E., Kiskinova, M. P., Kurdi, G., Manfredda, M., Masciovecchio, C., Mincigrucci, R., Nikolov, I. P., Pedersoli, E., Principi, E. & Sigalotti, P. (2014). *Opt. Express*, **22**, 12869–12879.

De Ninno, G., Gauthier, D., Mahieu, B., Ribič, P. R., Allaria, E., Cinquegrana, P., Danailov, M. B., Demidovich, A., Ferrari, E., Giannessi, L., Penco, G., Sigalotti, P. & Stupar, M. (2015). *Nat. Commun.* **6**, 8075.

Dhar, L., Rogers, J. A. & Nelson, K. A. (1994). *Chem. Rev.* **94**, 157–193.

Diels, J. C. & Rudolph, W. (2006). *Ultrashort Laser Pulse Phenomena*, 2nd ed. New York: Academic Press.

Düsterer, S., Rehders, M., Al-Shemmary, A., Behrens, C., Brenner, G., Brovko, O., Dell'Angela, M., Drescher, M., Faatz, B., Feldhaus, J., Frühling, U., Gerasimova, N., Gerken, N., Gerth, C., Golz, T., Grebentsov, A., Hass, E., Honkavaara, K., Kocharian, V., Kurka, M., Limberg, T., Mitzner, R., Moshammer, R., Plönjes, E., Richter, M., Rönsch-Schulenburg, J., Rudenko, A., Schlarb, H., Schmidt, B., Senftleben, A., Schneidmiller, E. A., Siemer, B., Sorgenfrei, F., Sorokin, A. A., Stojanovic, N., Tiedtke, K., Treusch, R., Vogt, M., Wieland, M., Wurth, W., Wesch, S., Yan, M., Yurkov, M. V., Zacharias, H. & Schreiber, S. (2014). *Phys. Rev. ST Accel. Beams*, **17**, 120702.

Emma, P., Akre, R., Arthur, J., Bionta, R., Bostedt, C., Bozek, J., Brachmann, A., Bucksbaum, P., Coffee, R., Decker, F.-J., Ding, Y., Dowell, D., Edstrom, S., Fisher, A., Frisch, J., Gilevich, S., Hastings, J., Hays, G., Hering, P., Huang, Z., Iverson, R., Loos, H., Messerschmidt, M., Miahnahri, A., Moeller, S., Nuhn, H.-D., Pile, G., Ratner, D., Rzepiela, J., Schultz, D., Smith, T., Stefan, P.,

Tompkins, H., Turner, J., Welch, J., White, W., Wu, J., Yocky, G. & Galayda, J. (2010). *Nat. Photon.* **4**, 641.
Feldhaus, J. (2010). *J. Phys. B*, **43**, 194002.
Ferrari, E., Spezzani, C., Fortuna, F., Delaunay, R., Vidal, F., Nikolov, I., Cinquegrana, P., Diviacco, B., Gauthier, D., Penco, G., Ribič, P. R., Roussel, E., Trovò, M., Moussy, J. B., Pincelli, T., Lounis, L., Manfredda, M., Pedersoli, E., Capotondi, F., Svetina, C., Mahne, N., Zangrando, M., Raimondi, L., Demidovich, A., Giannessi, L., De Ninno, G., Danailov, M. B., Allaria, E. & Sacchi, M. (2016). *Nat. Commun.* **7**, 10343.
Finetti, P., Höppner, H., Allaria, E., Callegari, C., Capotondi, F., Cinquegrana, P., Coreno, M., Cucini, R., Danailov, M. B., Demidovich, A., De Ninno, G., Di Fraia, M., Feifel, R., Ferrari, E., Fröhlich, L. V., Gauthier, D., Golz, T., Grazioli, C., Kai, Y., Kurdi, G., Mahne, N., Manfredda, M., Medvedev, N., Nikolov, I. P., Pedersoli, E., Penco, G., Plekan, O., Prandolini, M. J., Prince, K. C., Raimondi, L., Rebernik, P., Riedel, R., Roussel, E. L., Sigalotti, P., Squibb, R., Stojanovic, N., Stranges, S., Svetina, C., Tanikawa, T., Teubner, U., Tkachenko, V., Toleikis, S., Zangrando, M., Ziaja, B., Tavella, F. & Giannessi, L. (2017). *Phys. Rev. X*, **7**, 021043.
Foster, M. A., Turner, A. C., Sharping, J. E., Schmidt, B. S. M., Lipson, M. & Gaeta, A. L. (2006). *Nature (London)*, **441**, 960–963.
Fuchs, M., Trigo, M., Chen, J., Ghimire, S., Shwartz, S., Kozina, M., Jiang, M., Henighan, T., Bray, C., Ndabashimiye, G., Bucksbaum, P. H., Feng, Y., Herrmann, S., Carini, G. A., Pines, J., Hart, P., Kenney, C., Guillet, S., Boutet, S., Williams, G. J., Messerschmidt, M., Seibert, M. M., Moeller, S., Hastings, J. B. & Reis, D. A. (2015). *Nat. Phys.* **11**, 964–970.
Gahl, C., Azima, A., Beye, M., Deppe, M., Döbrich, K., Hasslinger, U., Hennies, F., Melnikov, A., Nagasono, M., Pietzsch, A., Wolf, M., Wurth, W. & Föhlisch, A. (2008). *Nat. Photon.* **2**, 165–169.
Gaižauskas, E., Steponkevičius, K. & Vaičaitis, V. (2016). *Phys. Rev. A*, **93**, 023813.
Glover, T. E., Fritz, D. M., Cammarata, M., Allison, T. K., Coh, S., Feldkamp, J. M., Lemke, H., Zhu, D., Feng, Y., Coffee, R. N., Fuchs, M., Ghimire, S., Chen, J., Shwartz, S., Reis, D. A., Harris, S. E. & Hastings, J. B. (2012). *Nature (London)*, **488**, 603–608.
Günther, C. M., Pfau, B., Mitzner, R., Siemer, B., Roling, S., Zacharias, H., Kutz, O., Rudolph, I., Schondelmaier, D., Treusch, R. & Eisebitt, S. (2011). *Nat. Photon.* **5**, 99–102.
Helml, W., Maier, A. R., Schweinberger, W., Grguraš, I., Radcliffe, P., Doumy, G., Roedig, C., Gagnon, J., Messerschmidt, M., Schorb, S., Bostedt, C., Grüner, F., DiMauro, L. F., Cubaynes, D., Bozek, J. D., Tschentscher, Th., Costello, J. T., Meyer, M., Coffee, R., Düsterer, S., Cavalieri, A. L. & Kienberger, R. (2014). *Nat. Photon.* **8**, 950–957.
Ishikawa, T., Aoyagi, H., Asaka, T., Asano, Y., Azumi, N., Bizen, T., Ego, H., Fukami, K., Fukui, T., Furukawa, Y., Goto, S., Hanaki, H., Hara, T., Hasegawa, T., Hatsui, T., Higashiya, A., Hirono, T., Hosoda, N., Ishii, M., Inagaki, T., Inubushi, Y., Itoga, T., Joti, Y., Kago, M., Kameshima, T., Kimura, H., Kirihara, Y., Kiyomichi, A., Kobayashi, T., Kondo, C., Kudo, T., Maesaka, H., Maréchal, X. M., Masuda, T., Matsubara, S., Matsumoto, T., Matsushita, T., Matsui, S., Nagasono, M., Nariyama, N., Ohashi, H., Ohata, T., Ohshima, T., Ono, S., Otake, Y., Saji, C., Sakurai, T., Sato, T., Sawada, K., Seike, T., Shirasawa, K., Sugimoto, T., Suzuki, S., Takahashi, S., Takebe, H., Takeshita, K., Tamasaku, K., Tanaka, H., Tanaka, R., Tanaka, T., Togashi, T., Togawa, K., Tokuhisa, A., Tomizawa, H., Tono, K., Wu, S., Yabashi, M., Yamaga, M., Yamashita, A., Yanagida, K., Zhang, C., Shintake, T., Kitamura, H. & Kumagai, N. (2012). *Nat. Photon.* **6**, 540.
Jiang, Y. H., Pfeifer, T., Rudenko, A., Herrwerth, O., Foucar, L., Kurka, M., Kühnel, K. U., Lezius, M., Kling, M. F., Liu, X., Ueda, K., Düsterer, S., Treusch, R., Schröter, C. D., Moshammer, R. & Ullrich, J. (2010). *Phys. Rev. A*, **82**, 041403.
Lutman, A. A., Ding, Y., Feng, Y., Huang, Z., Messerschmidt, M., Wu, J. & Krzywinski, J. (2012). *Phys. Rev. ST Accel. Beams*, **15**, 030705.
Maltezopoulos, T., Cunovic, S., Wieland, M., Beye, M., Azima, A., Redlin, H., Krikunova, M., Kalms, R., Frühling, U., Budzyn, F., Wurth, W., Föhlisch, A. & Drescher, M. (2008). *New J. Phys.* **10**, 033026.
Medvedev, N., Ziaja, B., Cammarata, M., Harmand, M. & Toleikis, S. (2013). *Contrib. Plasma Phys.* **53**, 347–354.
Mitzner, R., Siemer, B., Neeb, M., Noll, T., Siewert, F., Roling, S., Rutkowski, M., Sorokin, A. A., Richter, M., Juranic, P., Tiedtke, K., Feldhaus, J., Eberhardt, W. & Zacharias, H. (2008). *Opt. Express*, **16**, 19909.
Mitzner, R., Sorokin, A. A., Siemer, B., Roling, S., Rutkowski, M., Zacharias, H., Neeb, M., Noll, T., Siewert, F., Eberhardt, W., Richter, M., Juranic, P., Tiedtke, K. & Feldhaus, J. (2009). *Phys. Rev. A*, **80**, 025402.
Moshammer, R., Pfeifer, Th., Rudenko, A., Jiang, Y. H., Foucar, L., Kurka, M., Kühnel, K. U., Schröter, C. D., Ullrich, J., Herrwerth, O., Kling, M. F., Liu, X.-J., Motomura, K., Fukuzawa, H., Yamada, A., Ueda, K., Ishikawa, K. L., Nagaya, K., Iwayama, H., Sugishima, A., Mizoguchi, Y., Yase, S., Yao, M., Saito, N., Belkacem, A., Nagasono, M., Higashiya, A., Yabashi, M., Ishikawa, T., Ohashi, H., Kimura, H. & Togashi, T. (2011). *Opt. Express*, **19**, 21698.
Mukamel, S. (1995). *Principles of Nonlinear Optics and Spectroscopy*. Oxford University Press.
Nighan, W. L. Jr, Gong, T., Liou, L. & Fauchet, P. M. (1989). *Opt. Commun.* **69**, 339–344.
Raimondi, L., Svetina, C., Mahne, N., Cocco, D., Abrami, A., De Marco, M., Fava, C., Gerusina, S., Gobessi, R., Capotondi, F., Pedersoli, E., Kiskinova, M., De Ninno, G., Zeitoun, P., Dovillaire, G., Lambert, G., Boutu, W., Merdji, H., Gonzalez, A. I., Gauthier, D. & Zangrando, M. (2013). *Nucl. Instrum. Methods Phys. Res. A*, **710**, 131–138.
Ratner, D., Fry, A., Stupakov, G. & White, W. (2012). *Phys. Rev. ST Accel. Beams*, **15**, 030702.
Riedel, R., Al-Shemmary, A., Gensch, M., Golz, T., Harmand, M., Medvedev, N., Prandolini, M. J., Sokolowski-Tinten, K., Toleikis, S., Wegner, U., Ziaja, B., Stojanovic, N. & Tavella, F. (2013). *Nat. Commun.* **4**, 1731.
Roth, J. M., Murphy, T. E. & Xu, C. (2002). *Opt. Lett.* **27**, 2076–2078.
Schlotter, W. F., Sorgenfrei, F., Beeck, T., Beye, M., Gieschen, S., Meyer, H., Nagasono, M., Föhlisch, A. & Wurth, W. (2010). *Opt. Lett.* **35**, 372–374.
Shwartz, S., Fuchs, M., Hastings, J. B., Inubushi, Y., Ishikawa, T., Katayama, T., Reis, D. A., Sato, T., Tono, K., Yabashi, M., Yudovich, S. & Harris, S. E. (2014). *Phys. Rev. Lett.* **112**, 163901.
Tanaka, S., Chernyak, V. & Mukamel, S. (2001). *Phys. Rev. A*, **63**, 063405.
Tanaka, S. & Mukamel, S. (2002). *Phys. Rev. Lett.* **89**, 043001.
Walmsley, A. & Dorrer, C. (2009). *Adv. Opt. Photon.* **1**, 308.
Wöstmann, M., Mitzner, R., Noll, T., Roling, S., Siemer, B., Siewert, F., Eppenhoff, S., Wahlert, F. & Zacharias, H. (2013). *J. Phys. B*, **46**, 164005.
Ziaja, B., Jurek, Z., Medvedev, N., Thiele, R. & Toleikis, S. (2013). *High. Energ. Density Phys.* **9**, 462–472.